THE JOURNAL OF PHYSICAL CHEMISTRY C

Article

Synthesis and Optical and Magnetic Properties of Diluted Magnetic Semiconductor Zn$_{1-x}$Mn$_x$O Hollow Spherical Structures

X. X. Lin, Y. F. Zhu, and W. Z. Shen

J. Phys. Chem. C, **2009**, 113 (5), 1812-1817 • Publication Date (Web): 14 January 2009

Synthesis and Optical and Magnetic Properties of Diluted Magnetic Semiconductor $Zn_{1-x}Mn_xO$ Hollow Spherical Structures

X. X. Lin, Y. F. Zhu, and W. Z. Shen*

Laboratory of Condensed Matter Spectroscopy and Opto-Electronic Physics, Department of Physics, Shanghai Jiao Tong University, 1954 Hua Shan Road, Shanghai 200030, People's Republic of China

Received: November 18, 2008; Revised Manuscript Received: December 11, 2008

A simple chemical vapor deposition technique has been employed to realize $Zn_{1-x}Mn_xO$ hollow spherical structures with room temperature ferromagnetism. We propose a special experimental scheme for the appropriate growth temperature, which could not only realize effective evaporation of the source materials, but also make further vaporization of the Zn enclosed in the Mn-doped ZnO layer and avoid the formation of Mn-related oxides on the substrates. A series of controlled experiments have been carried out for better understanding the formation mechanism. The morphology, structure, and composition have been investigated by field-emission scanning electron microscopy, high-resolution transmission electron microscopy, X-ray diffraction, and energy dispersive X-ray analysis, indicating that Mn^{2+} was successfully substituted into the Zn^{2+} site. Raman results show an additional mode (520−530 cm^{-1}) in the doped samples due to the lattice defects triggered by Mn doping. Multipeak Gaussian fitting of the photoluminscence spectra exhibits an emission related to the d−d transition of Mn^{2+} from the ground state $^6A_1(G)$ to the excited state $^4E(G)$. The origin of the room temperature ferromagnetism has been attributed to the magnetic coupling between Mn atoms.

I. Introduction

Since the theoretical prediction of room temperature ferromagnetism in transitional metal-doped ZnO and GaN by Dietl et al.,[1] ZnO-based diluted magnetic semiconductors have been extensively studied for the potential application in spintronic devices and magneto-optic components.[2−5] Experimentally, room temperature ferromagnetism has been reported in V-,[6] Co-,[7] Ni-,[8] Fe-,[9] Cu-,[10] and Mn-doped[11−16] ZnO systems. Among all the transitional metal-doped ZnO systems, Mn doping has its own advantage because of its intrinsic physical properties of large magnetic moment due to a half-filled 3d band and relatively small ionic radius difference between Mn^{2+} (0.66 Å) and host cation Zn^{2+} (0.60 Å).[4,5,13]

During the past 5 years, Mn-doped ZnO systems with room temperature ferromagnetism have been successfully realized through methods such as a soft chemical route,[11] a solution-based process,[12] a rheological phase reaction precursor method,[13] rf magnetron sputtering,[14] and chemical vapor deposition.[15−18] Until now, most groups have devoted their efforts to Mn-doped ZnO films,[14] nanorods,[16] and nanoparticles.[13] To the best of our knowledge, there is no report on the Mn-doped ZnO hollow spherical structures with room temperature ferromagnetism. Actually, the synthesis and optical and magnetic properties of hollow micro- and nanospherical structures are very important due to their broad potential applications in photonic crystals, catalysts, sensors, artificial cells, nanoscale chemical reactors, energy-storage media, drug-delivery carriers, etc.[19] Presently, the two main techniques to synthesize pure ZnO hollow spherical structures are a thermal evaporation process and a template hydrothermal method. The former generally involves high growth temperature (typically ≥750 °C)[20a,b] that leads to a poor solubility of Mn in the ZnO system and aggregation of secondary phases.[5] The latter depends on sacrificing templates and requires a complicated synthetic procedure, which makes a successful Mn doping more difficult. Therefore, it is necessary to develop a feasible and simple method to prepare Mn-doped ZnO hollow spherical structures.

In this paper, we report on the successful synthesis of $Zn_{1-x}Mn_xO$ hollow spherical structures with room temperature ferromagnetism through a simple chemical vapor deposition technique under atmospheric pressure. Through analyzing the effect of growth temperature and reaction time on the morphology of the as-prepared products, we have demonstrated that the key factor for success lies in the appropriate growth temperature. Since the melting points of zinc (Zn) power and manganese chloride tetrahydrate ($MnCl_2 \cdot 4H_2O$) are about 420 and 650 °C, respectively, the source materials could be effectively evaporated at 600−700 °C. We arrange the substrate 30 cm away from the center of the furnace, its temperature (∼500 °C) is lower than that of reaction (600−700 °C) to avoid the formation of Mn-related oxides, but higher than the melting point of Zn to vaporize into Zn steam. We have also studied in detail the structural, optical, and magnetic properties of the obtained Mn-doped ZnO hollow spherical structures with different Mn contents grown at 650 °C and attributed the room temperature ferromagnetism to the magnetic coupling between Mn atoms.

II. Experimental Details

$Zn_{1-x}Mn_xO$ hollow spherical structures were synthesized by the chemical vapor deposition method in a horizontal tube furnace in air. The experimental setup is schematically demonstrated in Figure 1a. Zn (99.99% purity) and $MnCl_2 \cdot 4H_2O$ powders (99.99% purity) were first mixed at an appropriate proportion, and the mixture was loaded into a ceramic boat placed at the end of a one-end sealed quartz tube with a 2 cm diameter. Si (100) substrates were placed about 30 cm away from the source materials to receive the products. Then the quartz tube was inserted into the horizontal tube furnace, placing

* Corresponding author. Fax: +86-21-54747552. E-mail: wzshen@sjtu.edu.cn.

10.1021/jp810134h CCC: $40.75
Published on Web 01/14/2009

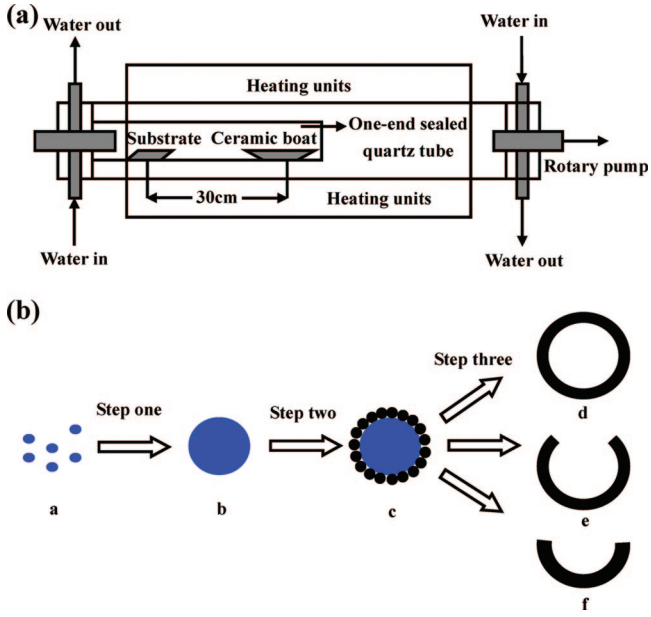

Figure 1. (a) Schematic diagram of the experimental apparatus for the growth of $Zn_{1-x}Mn_xO$ hollow spherical structures. (b) Schematic illustration of the formation of three type $Zn_{1-x}Mn_xO$ hollow spherical structures: a, Mn-doped Zn spheres; b, Mn-doped Zn spheres assembled on silicon substrate; c, oxidation of the spheres to form a thin layer of Mn-doped ZnO nanoparticles; evolvement into (d) $Zn_{1-x}Mn_xO$ shell at 600 °C, (e) $Zn_{1-x}Mn_xO$ hollow structures at 650 °C, and (f) $Zn_{1-x}Mn_xO$ hemispheric structures at 700 °C.

the sealed end at the center of the furnace tube. After that, the tube furnace was evacuated by using a mechanical rotary pump to remove the residual oxygen and heated to appropriate temperatures of 600, 650, and 700 °C, respectively, at a rate of 10 deg/min. As soon as it reached the desired temperature, we stopped the evacuation of the mechanical rotary pump, slowly introduced air into the furnace system, and kept the samples under atmospheric pressure for 2 min. Finally, we maintained the total growth time for 30, 60, 120, and 180 min, respectively, according to different experimental purposes. Due to the temperature gradient of the tube furnace, the Si substrate temperature was around 500 °C. The yellowish powder on the Si substrate could be obtained after the furnace was cooled to room temperature naturally.

The morphology and structure of the $Zn_{1-x}Mn_xO$ hollow spherical structures were characterized by using a field emission scanning electron microscope (FE-SEM; Philips XL30FEG) with an accelerating voltage of 5 kV, high resolution transmission electron microscope (HRTEM) (JEOL JEM-2100F), and X-ray diffraction (XRD) Bruker/D8 Discover diffractometer with GADDS equipped with a Cu Kα source ($\lambda = 1.5406$ Å). Energy dispersive X-ray (EDX) analysis was also performed during the FE-SEM observation and the selected area electron diffraction (SAED) was processed during HRTEM measurements. The micro-Raman in the backscattering geometry and photoluminscence (PL) spectra were recorded at room temperature by a Jobin Yvon LabRAM HR800UV micro-Raman system under an Ar^+ (514.5 nm) and a He−Cd (325.0 nm) laser excitation, respectively. The magnetic properties of the samples were obtained by a physical property measurement system (PPMS-12). The electron paramagnetic resonance (EPR) spectra were collected on a Bruker EMX-8/2.7 electro-spin-resonance spectrometer system at room temperature.

III. Results and Discussion

Panels a−c in Figure 2 show the typical FE-SEM images of the as-prepared products at 600, 650, and 700 °C for 120 min. The EDX analysis shown below indicates that the molar ratio of Mn in every sample is $x = 1.26\%$. It is clearly seen that all the samples are accumulated by nanoparticles several hundred nanometers in size. We can observe that the structures obtained at 600 °C exhibit sealed spherical shells. With the increase of reaction temperature, the products are evolved into partially opened spherical shells at 650 °C and hemispheric shells at 700 °C. To exploit the influence of the reaction time on the morphology of the synthesized products, we have also prepared the hollow spherical structures with Mn content 1.26% at 700 °C for 30, 60, and 180 min, respectively. Panels d−f in Figure 2 present the typical morphology of the as-prepared products at 700 °C with different reaction times. It is obvious that the structures of the products were reinforced and the sizes of the products were increased with the extension of time.

TEM measurements have been carried out for structural investigation of the obtained hollow spherical structure. Figure 2g shows the typical TEM image of a single hollow spherical structure produced at 650 °C for 120 min with the Mn content 1.26%. The result confirms that the as-prepared sample is the hollow spherical structure since the images contain a light inner part and a relatively darker outer spherical part. Figure 2h is the lattice resolved HRTEM image of the selected Mn-doped nanoparticle indicated in Figure 2g with a red rectangular. The lattice fringe is about 0.26 nm, which corresponds to the [0002] crystal planes of wurzite ZnO. It also indicates that the nanoparticle is single crystalline and the growth direction is perpendicular to the [0001] plane. The corresponding SAED pattern illustrated in Figure 2i also exhibits the same phenomenon.

On the basis of the above experimental observations and the previously reported results on the synthesis of pure ZnO hollow microspheres,[20] we suggest that the possible growth mechanism can be described as illustrated in Figure 1b. In step one, the Zn and Mn vapor generated by the melted mixture powers assembled into Mn-doped Zn spheres on the low-temperature Si substrates. In step two, the outside layer of the Mn-doped Zn spheres experienced a quick oxidation and a sparse layer of Mn-doped ZnO nanoparticles was formed on the Mn-doped Zn spheres after introducing air into the furnace. In step three, the inner Mn-doped Zn was further vaporized and deposited on and between the existing Mn-doped ZnO nanoparticles. In this step, the substrate temperature is the key point to realize the synthesis of hollow spherical structures with different morphology. When the substrate temperature is higher than the melting point of Zn (about 420 °C), the Mn-doped ZnO layer enclosed Zn was partially vaporized into Zn steam. At 600 °C we consider that the pressure generated by the Zn steam is equivalent to that of the atmosphere, therefore, it is formed into sealed spherical shell with the increment of reaction time (Figure 2a). The pressure generated by the Zn steam intensifies with the increase of temperature: the weakest part of the synthesized Mn-doped ZnO layer is apt to break up to realize an equivalent pressure in and outside the Mn-doped ZnO layer. The force due to the pressure difference strengthens with increasing temperature, resulting in a larger broken area or even destruction of the whole structure at higher temperatures. Therefore, the products grew into partially broken shell (Figure 2b) or hemispheric shell (Figure 2c) at different temperatures.

The observation of the morphology variation with the reaction time in panels d−f in Figure 2 gives clear support for the above growth mechanism. Loose Mn-doped ZnO hemispheric struc-

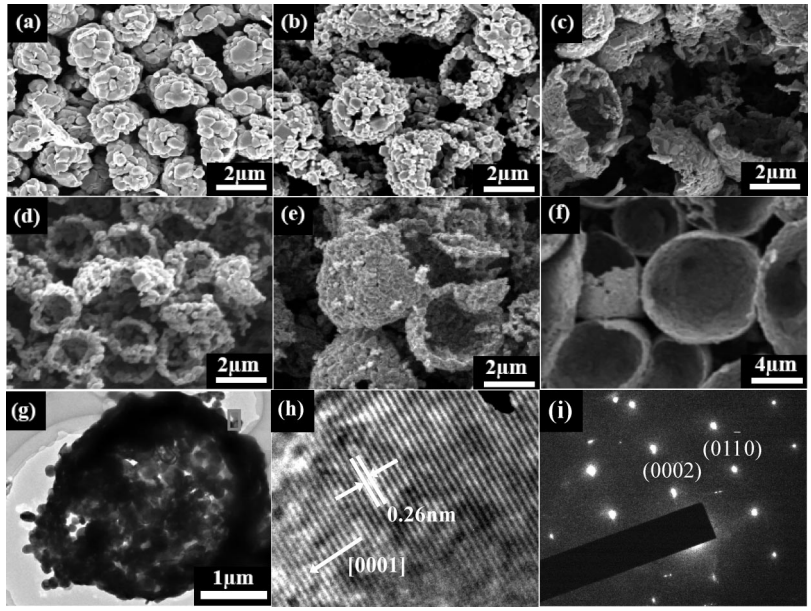

Figure 2. (a−c) FE-SEM images of $Zn_{1-x}Mn_xO$ hollow spherical structures with $x = 1.26\%$ grown for 120 min at 600, 650, and 700 °C, respectively. (d−f) FE-SEM images of $Zn_{1-x}Mn_xO$ hollow spherical structures with $x = 1.26\%$ grown at 700 °C for 30, 60, 180 min, respectively. (g−i) TEM image, HRTEM image [the selected area is indicated with a red rectangular in part g], and the corresponding SEAD pattern of $Zn_{1-x}Mn_xO$ hollow spherical structures with $x = 1.26\%$ grown at 650 °C for 120 min.

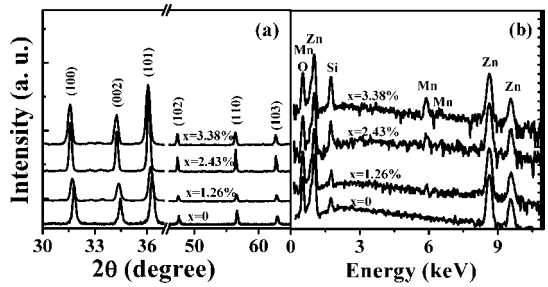

Figure 3. (a) XRD pattern and (b) EDX spectra of undoped ZnO and $Zn_{1-x}Mn_xO$ hollow spherical structures grown at 650 °C for 120 min with Mn content $x = 1.26\%$, 2.43%, and 3.38%, respectively. The EDX intensity is the experimental intensity on a base-2 logarithmic scale.

tures were obtained at 700 °C for 30 min (Figure 2d), indicating that at an early stage a sparse layer of Mn-doped ZnO nanoparticles was synthesized. Since it was produced at 700 °C, the inner pressure originating from the Mn-doped Zn steam was very large and the rest of the Mn-doped Zn could be evaporated very quickly. With the extension of the reaction time, the Mn-doped Zn vapor was deposited on and between the existing Mn-doped ZnO nanoparticles and oxidized into Mn-doped ZnO nanoparticles too, leading to the experimental observation of the compact and enlarged hemispheric structures shown in panels e and f in Figure 2.

XRD and EDX measurements have been performed on the structure and composition of the obtained $Zn_{1-x}Mn_xO$ hollow spherical structure with different Mn contents synthesized at 650 °C for 120 min. We use the undoped ZnO produced under the same growth condition as a reference. It could be observed from Figure 3a that six prominent XRD peaks correspond to (100), (002), (101), (102), (110), and (103) crystal planes of hexagonal ZnO according to the standards of the Joint Committee on Powder Diffraction Standards. This result is coincident with the HRTEM observation that the product is the wurtize ZnO structrure. The experimental fact that we cannot observe diffraction features from metallic Mn, Mn oxides, or other zinc manganese phases suggests that Mn^{2+} is successfully substituted at the Zn^{2+} sites and the samples are in the single phase. This is reasonable since our design of substrate temperature (∼500 °C) is lower than that of reaction (600−700 °C) to avoid the formation of Mn-related oxides. Moreover, it is noted that with the increase of Mn content the XRD peaks of Mn-doped samples have constantly shifted to lower scattering angle, indicating an enhancement of the lattice constant that can be attributed to the fact that the ionic radius of Mn^{2+} (0.66 Å) is larger than that of Zn^{2+} (0.60 Å).[13] Using the Scherrer formula, we can learn that the *a*-axis and *c*-axis lattice constants increase from 3.243 and 5.204 Å for undoped ZnO to 3.261 and 5.225 Å for the Mn-doped ZnO hollow spherical structure with Mn content $x = 3.38\%$, respectively. The corresponding EDX spectra are shown in Figure 3b. The exhibited intensity is the experimental intensity on a base-2 logarithmic scale. The results indicate that the as-prepared $Zn_{1-x}Mn_xO$ hollow spherical structures are composed of Zn, Mn, and O elements while the signal of Si originates from the Si substrate. From the atomic ratio of Mn to Zn in the EDX spectra, we can determine the molar ratio of Mn (x=[Mn]/([Zn] + [Mn]) in $Zn_{1-x}Mn_xO$ hollow spherical structures to be $x = 0$, 1.26%, 2.43%, and 3.38%, respectively.

Figure 4 presents the room temperature Raman spectra of both the undoped ZnO and the $Zn_{1-x}Mn_xO$ hollow spherical structures with different Mn contents synthesized at 650 °C for 120 min. The sharpest and strongest peak around 437 cm^{-1} can be assigned to the nonpolar optical phonon E_2(high) mode of ZnO. It is related to the motion of oxygen atoms and is a typical Raman active branch of wurtzite ZnO.[21,22] The presence of the E_2(high) mode in all four samples indicates the hexagonal wurtzite structure, which is in good agreement with the HRTEM and XRD observations. In the undoped ZnO sample the E_1[longitudinal-optical (LO)] mode is approximately at ∼580 cm^{-1}. With the increase of the Mn content, the E_1(LO) mode shifts to lower frequency. In comparison with the Raman spectrum of pure ZnO, an additional mode that is indicated as

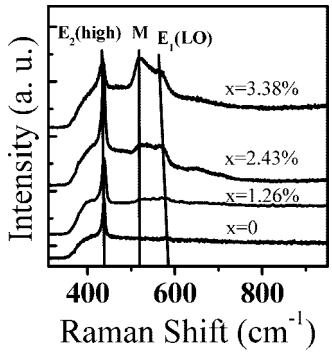

Figure 4. Room temperature Raman spectra of undoped ZnO and $Zn_{1-x}Mn_xO$ hollow spherical structures grown at 650 °C for 120 min with Mn content $x = 1.26\%$, 2.43%, and 3.38%, respectively.

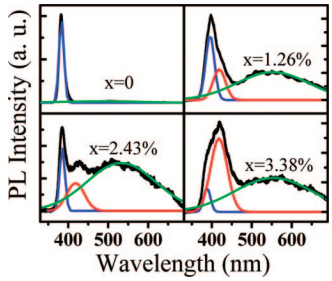

Figure 5. Room temperature PL spectra of undoped ZnO and $Zn_{1-x}Mn_xO$ hollow spherical structures grown at 650 °C for 120 min with Mn content $x = 1.26\%$, 2.43%, and 3.38%, respectively.

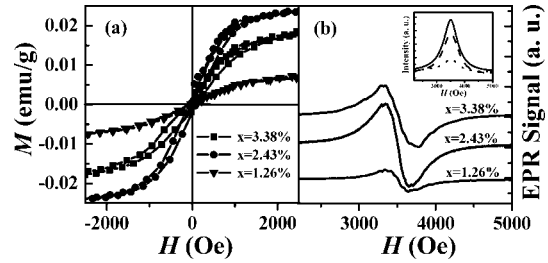

Figure 6. (a) Room temperature magnetic hysteresis loops ($M-H$ curves) and (b) EPR spectra of $Zn_{1-x}Mn_xO$ hollow spherical structures grown at 650 °C for 120 min with Mn content $x = 1.26\%$, 2.43%, and 3.38%, respectively. The inset in part b shows the integration of the three original EPR signals, where the solid, dashed, and dotted curves represent the as-prepared sample with Mn content $x = 2.43\%$, 3.38%, and 1.26%, respectively.

M around 520−530 cm^{-1} is observed in the Mn-doped ZnO samples. It can be attributed to the lattice defects triggered by the incorporation of Mn^{2+} into the host lattice.[23−25] From Figure 4, it is obvious that the intensity ratio of the additional peak to the E_2(high) peak increases from 0 to ∼1.0 with the Mn content from $x = 0$ to 3.38%, suggesting that the lattice defects are introduced gradually by the Mn doping. In our produced samples, the room temperature Raman spectra did not show a vibration mode related to Zn_2MnO_4 at 663 cm^{-1},[26] i.e., non-secondary phase in the $Zn_{1-x}Mn_xO$ hollow spherical structures. This result is also in agreement with the XRD studies in Figure 3a and the experimental design.

We further perform the PL spectroscopy to explore the optical properties of the $Zn_{1-x}Mn_xO$ hollow spherical structures. Figure 5 displays the room temperature PL spectra of the undoped ZnO and the doped ZnO system synthesized at 650 °C for 120 min with different Mn contents. We notice that all the samples contain a strong ultraviolet (UV) peak at ∼386 nm. That is, Mn doping does not change the peak position, which is consistent with the results reported in the literature.[27,28] However, it is obvious that the near band UV emission peak broadens with the increase of the Mn content. A multipeak Gaussian fitting has been employed to investigate the PL spectra in the range of 330 to 700 nm, where an additional emission peak at around 417 nm appears in the Mn-doped samples, in agreement with other reported experimental and theoretical results.[29−32] Some reports have also pointed out the near band UV emission can be attributed to the interstitial Zn.[33] Since the XRD studies have already shown that there is no Zn signal in the produced samples and the EDX results suggest the atomic ration of Zn to O is ∼1, we can exclude the influence of the interstitial Zn. Using the integrated intensity ratio [$I_{\text{additional emission}}/I_{\text{UV}}$] of the additional emission (marked as the red curves) to ZnO UV peak (marked as the blue ones) as a function of Mn content x, we can obtain that the value of $I_{\text{additional emission}}/I_{\text{UV}}$ increases from 0 to ∼5 for $x = 0$ to 3.38%. Mizokawa et al.[32] have calculated the d−d transition energy levels of Mn^{2+} ion in Mn-doped ZnO films using the MnY_4 cluster model (Y is an anion) and stated that the energy difference between the ground state $^6A_1(G)$ and the excited state $^4E(G)$ is 2.97 eV (equivalent to 417 nm). Therefore, we here attribute this additional peak to the d−d transition of Mn^{2+} from the ground state $^6A_1(G)$ to the excited state $^4E(G)$. In a word, the increased value of $I_{\text{additional emission}}/I_{\text{UV}}$ shows the intensified d−d transition of Mn^{2+} ion with the increase of Mn content and the additional emission peak gave clear evidence to the incorporation of the Mn^{2+} to the ZnO host lattice.

The broad visible luminescence (marked as the green curves in Figure 5) is generally believed to be associated with the recombination of a photogenerated hole with the singly ionized oxygen vacancy and its intensity could be used as an indicator of the oxygen vacancy concentration in ZnO.[17,34] From Figure 5 the undoped ZnO has a negligible green band emission indicating a high quality of the synthesized ZnO with low oxygen vacancy concentration. The strong green band emission in Mn-doped ZnO hollow spherical structures can be attributed to the oxygen vacancies introduced by Mn^{2+} incorporation into the host lattice. The intensity ratio of the green band emission to the ZnO UV peak enhances from ∼0.02 to ∼1.50 for $x = 0$ to 3.38%, demonstrating that the Mn doping strongly increases the concentration of oxygen vacancy. This result is consistent with the above Raman observation that the lattice defects are generated gradually with the Mn doping.

We finally investigate the magnetic properties of the $Zn_{1-x}Mn_xO$ hollow spherical structures. The hysteresis loops have also been measured at room temperature for the obtained products synthesized at 650 °C for 120 min. Figure 6a shows the magnetization (M) versus magnetic field (H) ($M-H$) curves of the Mn-doped ZnO hollow spherical structures in the field range of 0 ∼ ±2500 Oe. It could be observed that all three samples are ferromagnetic at 300 K with a coercivity $H_C \approx 70 \pm 5$ Oe. Since Mn-related oxides such as MnO, MnO_2, and Mn_2O_3 are antiferromagnetic while Mn_3O_4 is ferromagnetic below 45 K,[35] the observation of room temperature ferromagnetism in the present $Zn_{1-x}Mn_xO$ hollow spherical structures can also exclude the presence of the above-mentioned oxides, and the room temperature magnetism is related only to the incorporation of Mn^{2+} ion into the host lattice. There are some reports on ferromagnetism Mn-doped ZnO films,[14] nanorods,[16] and nanoparticles;[25] however, Mn-doped ZnO hollow spherical

structures have not been realized before. Compared with the previous reported results, although the hollow spherical structures prepared by the present method demonstrated similar ferromagnetism property, the successful synthesis of ferromagnetism hollow spherical structures is very important from the application point of view due to their unique hollow geometrical shapes.

It is seen from $M-H$ curves that the sample with the largest Mn content ($x = 3.38\%$) does not demonstrate the highest saturation magnetization. Theoretical calculation has revealed that Mn-doped ZnO thin films with higher Mn content results in a shorter distance of the magnetic coupling between Mn atoms, which is energetically favorable for Mn^{2+} ions to obtain antiferromagnetic state.[36] Therefore, when ZnO was doped with low Mn content, Mn^{2+} ions having no preference in the substituted Zn^{2+} site of the host lattice, the distance of the magnetic coupling between Mn^{2+} ions is long enough to induce a weak ferromagnetic interaction between the neighboring Mn^{2+} ions. The increase in Mn content intensifies such ferromagnetic interaction and reaches its largest in the present product at the Mn content of 2.43%. Further increment in Mn content leads to the arrangement of the antiferromagnetic moment and decreases the saturation magnetization. Mi et al.[14] have also reported such phenomenon in Mn-doped films where the maximum of average moment per Mn^{2+} ions was observed in films with 2.2% Mn content. We can therefore attribute the room temperature ferromagnetism of the $Zn_{1-x}Mn_xO$ hollow structures to the magnetic coupling between Mn atoms. Furthermore, it should be pointed out that the largest saturation magnetization in ZnO with 2.43% Mn content is only ~0.024 emu/g (0.122 μ_B/Mn). This value is much smaller than the theoretical value of ~5 μ_B/Mn for a free Mn^{2+} ion, which can be attributed to the antiferromagnetic superexchange interactions between adjacent Mn^{2+} ions.[17,23]

EPR measurements give further evidence for the incorporation of Mn^{2+} ions into the host lattice. Figure 6b shows the typical room temperature EPR results of the three doped samples. It could be observed that there are no hyperfine lines in the broad EPR signals, which confirms the successful incorporation of Mn^{2+} into the Zn sites.[13,37] From the integration intensity of the three original EPR signals (the inset of Figure 6b), we can obtain that the sample with 2.43% Mn content exhibits the strongest overall ferromagnetic interaction. The results are also in agreement with the variation of saturation magnetization shown in Figure 6a.

IV. Conclusions

In summary, we have developed a simple chemical vapor deposition technique to achieve $Zn_{1-x}Mn_xO$ hollow spherical structures with room temperature ferromagnetism. The source materials of Zn and $MnCl_2 \cdot 4H_2O$ powders were placed at the center of the tube furnace while the products were received on the Si substrates 30 cm away. This experimental scheme could not only realize effective evaporation of the source materials at 600−700 °C, but also allow further vaporization of the Zn enclosed in the Mn-doped ZnO layer and avoid the formation of Mn-related oxides on the substrates (around 500 °C). Furthermore, we introduced air into the furnace until it reached the desired temperature, i.e., the process of oxidation was not started until the Mn-doped Zn spheres were shaped. The morphology and size of the as-prepared products can be well controlled via proper regulation of the growth temperature and reaction time. We have employed the TEM, EDX, XRD, Raman, and PL to demonstrate that the hollow spherical structures are composed of single crystalline Mn-doped ZnO nanoparticles with wurtzite structure and confirm that Mn^{2+} ions are successfully incorporated into the host lattice. All the prepared samples exhibit room temperature ferromagnetism, which has been attributed to the magnetic coupling between Mn atoms. The method presented in this paper is a versatile strategy to fabricate other transitional metal-doped ZnO hollow spherical structures.

Acknowledgment. This work was supported by the Natural Science Foundation of China under contracts 10734020 and 10674094, National Major Basic Research Project of 2006CB921507, National Minister of Education Program of IRT0524, and Shanghai Municipal Key Project of 08XD14022.

References and Notes

(1) Dietl, T.; Ohno, H.; Matsukura, F.; Gilbert, J.; Ferrand, D. *Science* **2000**, *287*, 1019.
(2) Sluiter, M. H. F.; Kawazoe, Y.; Sharma, P.; Inoue, A.; Raju, A. R.; Rout, C.; Waghmare, U. V. *Phys. Rev. Lett.* **2005**, *94*, 187204.
(3) Sharmai, P.; Guptai, A.; Rao, K. V.; Owens, F. J.; Sharma, R.; Ahuja, R.; Guillen, J. M. O.; Johansson, B.; Gehring, G. A. *Nat. Mater.* **2003**, *2*, 673.
(4) Sato, K.; Yoshida, H. K. *Semicond. Sci. Technol.* **2002**, *17*, 367.
(5) Mandal, S. K.; Das, A. K.; Nath, T. K.; Karmakar, D. *Appl. Phys. Lett.* **2006**, *89*, 144105.
(6) Hong, N. H.; Sakai, J.; Hassini, A. *J. Appl. Phys.* **2005**, *97*, 10D312.
(7) Jayakumar, O. D.; Gopalakrishnan, I. K.; Kulshreshtha, S. K. *Adv. Mater.* **2006**, *18*, 1857.
(8) Schwartz, D. A.; Kittilstved, K. R.; Gamelin, D. R. *Appl. Phys. Lett.* **2004**, *85*, 1395.
(9) Karmakar, D.; Mandal, S. K.; Kadam, R. M.; Paulose, P. L.; Rajarajan, A. K.; Nath, T. K.; Das, A. K.; Dasgupta, I.; Das, G. P. *Phys. Rev. B* **2007**, *75*, 144404.
(10) Herng, T. S.; Lau, S. P.; Yu, S. F.; Yang, H. Y.; Wang, L.; Tanemura, M.; Chen, J. S. *Appl. Phys. Lett.* **2007**, *90*, 032509.
(11) Barick, K. C.; Aslam, M.; Dravid, V. P.; Bahadur, D. *J. Phys. Chem. C* **2008**, *112*, 15163.
(12) Guo, Y.; Cao, X. B.; Lan, X. M.; Zhao, C.; Xue, X. D.; Song, Y. Y. *J. Phys. Chem. C* **2008**, *112*, 8832.
(13) Cong, C. J.; Liao, L.; Li, J. C.; Fan, L. X.; Zhang, K. L. *Nanotechnology* **2006**, *17*, 1520.
(14) Mi, W. B.; Bai, H. L.; Liu, H.; Sun, C. Q. *J. Appl. Phys.* **2007**, *101*, 023904.
(15) Baik, J. M.; Lee, J.-L. *Adv. Mater.* **2005**, *17*, 2745.
(16) Yan, H. L.; Zhong, X. L.; Wang, J. B.; Huang, G. J.; Ding, S. L.; Zhou, G. C.; Zhou, Y. C. *Appl. Phys. Lett.* **2007**, *90*, 082503.
(17) Yan, W. S.; Sun, Z. H.; Liu, Q. H.; Li, Z. R.; Pan, Z. Y.; Wang, J.; Wei, S. Q. *Appl. Phys. Lett.* **2007**, *91*, 062113.
(18) Roy, V. A. L.; Djurišić, A. B.; Liu, H.; Zhang, X. X.; Leung, Y. H.; Xie, M. H.; Gao, J.; Lui, H. F.; Surya, C. *Appl. Phys. Lett.* **2004**, *84*, 756.
(19) (a) Zhu, Y. F.; Fan, D. H.; Shen, W. Z. *J. Phys. Chem. C* **2008**, *112*, 10402. (b) Liu, Y.; Chu, Y.; Zhuo, Y.; Dong, L.; Li, L.; Li, M. *Adv. Funct. Mater.* **2007**, *17*, 933. (c) Lou, X. W.; Yuan, C.; Rhoades, E.; Zhang, Q.; Archer, L. A. *Adv. Funct. Mater.* **2006**, *16*, 1679. (d) Noble, P. F.; Cayre, O. J.; Alargova, R. G.; Velev, O. D.; Paunov, V. N. *J. Am. Chem. Soc.* **2004**, *126*, 8092.
(20) (a) Gao, P. X.; Wang, Z. L. *J. Am. Chem. Soc.* **2003**, *125*, 11299. (b) Shen, G. Z.; Bando, Y. S.; Lee, C.-J. *J. Phys. Chem. B* **2005**, *109*, 10578. (c) Lu, H. B.; Liao, L.; Li, J. C.; Wang, D. F.; He, H.; Fu, Q.; Xu, L.; Tian, Y. *J. Phys. Chem. B* **2006**, *110*, 23211.
(21) Cao, B. Q.; Cai, W. P.; Zeng, H. B.; Duan, G. T. *J. Appl. Phys.* **2006**, *99*, 073516.
(22) Ashkenov, N.; Mbenkum, B. N.; Bundesmann, C.; Riede, V.; Lorenz, M.; Spemann, D.; Kaidashev, E. M.; Kasic, A.; Schubert, M.; Grundmann, M.; Wagner, G.; Neumann, H.; Darakchieva, V.; Arwin, H.; Monemar, B. *J. Appl. Phys.* **2003**, *93*, 126.
(23) Xu, H. Y.; Liu, Y. C.; Xu, C. S.; Liu, Y. X.; Shao, C. L.; Mu, R. *J. Chem. Lett.* **2006**, *124*, 074707.
(24) Venkataraj, S.; Ohashi, N.; Sakaguchi, I.; Adachi, Y.; Ohgaki, T. *J. Appl. Phys.* **2007**, *102*, 014905.
(25) Wang, J. B.; Huang, G. J.; Zhong, X. L.; Sun, L. Z.; Zhou, Y. C. *Appl. Phys. Lett.* **2006**, *88*, 252502.
(26) Wang, J. B.; Zhong, H. M.; Li, Z. F.; Lu, W. *J. Appl. Phys.* **2005**, *97*, 086105.
(27) Ronning, C.; Gao, P. X.; Ding, Y.; Wang, Z. L. *Appl. Phys. Lett.* **2004**, *84*, 783.

(28) Philipose, U.; Nair, S. V.; Trudel, S.; Souza, C. F.; Aouba, S. *Appl. Phys. Lett.* **2006**, *88*, 263101.
(29) Nakayama, M.; Tanaka, H.; Masuka, K.; Fukushima, T.; Ashida, A.; Fujimura, N. *Appl. Phys. Lett.* **2006**, *88*, 241908.
(30) Xu, C. X.; Sun, X. W.; Dong, Z. L.; Tan, S. T.; Cui, Y. P.; Wang, B. P. *J. Appl. Phys.* **2005**, *98*, 113513.
(31) Jin, Z. W.; Yoo, Y. Y.; Sekiguchi, T.; Chikyow, T. *Appl. Phys. Lett.* **2003**, *83*, 39.
(32) Mizokawa, T.; Nambu, T.; Fujimori, A.; Fukumura, T.; Kawasaki, M. *Phys. Rev. B* **2002**, *65*, 085209.
(33) (a) Cao, B. Q.; Cai, W. P.; Zeng, H. B. *Appl. Phys. Lett.* **2006**, *88*, 161101. (b) Zeng, H. B.; Cai, W. P.; Hu, J. L.; Liu, P. S. *J. Phys. Chem. B* **2005**, *109*, 18260. (c) Zeng, H. B.; Cai, W. P.; Hu, J. L.; Duan, G. T.; Liu, P. S.; Li, Y. *Appl. Phys. Lett.* **2006**, *88*, 171910.
(34) Vanheusden, K.; Warren, W. L.; Seager, C. H.; Tallant, D. K.; Voigt, J. A.; Gnade, B. E. *J. Appl. Phys.* **1996**, *79*, 7983.
(35) Norton, D. P.; Pearton, S. J.; Hebard, A. F.; Theodoropoulou, N.; Boatnr, L. A.; Wilson, R. G. *Appl. Phys. Lett.* **2003**, *82*, 239.
(36) Wang, Q.; Sun, Q.; Rao, B. K.; Jena, P. *Phys. Rev. B* **2004**, *69*, 233310.
(37) Liu, J. J.; Wang, K.; Yu, M. H.; Zhou, W. L. *J. Appl. Phys.* **2007**, *102*, 024301.

JP810134H